Charge transfer in the non-covalent functionalization of carbon nanotubes

Olayinka O. Ogunro and Xiao-Qian Wang*

We have performed force field-based molecular dynamics and first principles density functional calculations on porphyrins and metalloporphyrins interacting with single-walled carbon nanotubes. The flattening of the porphyrin macrocycle is indicative of the self-assembly of these aromatic structures onto carbon nanotubes. An analysis of the charge distributions for conduction and valence bands reveals a distinct charge transfer behavior from the porphyrin macrocycle to the metallic or semiconducting tubes that sheds considerable light on the experimentally observed selectivity of semiconducting nanotubes.

The nano forms of carbon, fullerenes, nanotubes and graphene are important building materials that cross all disciplines of science.[1–3] The supramolecular functionalization of single-walled carbon nanotubes (SWNTs) has recently attracted a great deal of attention because it exploits the surface chemistry of the nanotubes *via* π–π interactions and preserves the integrity of the electronic structure. Recent research has demonstrated the self-assembly of a variety of macromolecules, nanoaggregates and biomaterials on the surface of SWNTs.[1–3] Molecules, such as porphyrin, pyrene or flavin derivatives, self-assemble onto semiconducting tubes, revealing a convenient way to separate these from metallic examples.[1–8] Despite the abundance of experimental work on the adsorption of aromatic molecules, the nature of this intriguing type-selectivity is not fully understood. As the debundling of carbon nanotubes remains one of the foremost technological barriers to the realization of their potential applications, a theoretical understanding of the interactions, structure and physical properties of porphyrins with SWNTs is highly desirable.

In order to gain a better understanding of the interfacial chemistry and dispersion mechanism, we have employed a combination of force field-based molecular dynamics (MD) and first principles density functional calculations to investigate the structural and electronic properties of porphyrin-functionalized SWNTs. Force field-based MD is used to pre-screen molecular geometries, and first principles calculations are employed to determine the electronic structure of the nanohybrid. A fundamental issue is how non-covalent interactions affect the conformation of the porphyrin macrocycle, as these macromolecules possess flat planar geometries that are spontaneously attracted to the side walls of SWNTs, forming a host–guest nanohybrid. This type of functionalization

has a direct impact on the selectivity of nanotubes. Our results show that the π–π interaction between the porphyrin and the SWNT manifests itself *via* a flattening of the porphyrin macrocycle. Metalloporphyrins, as exemplified by Zn-porphyrin, have a less flattened conformation as compared to that of the free porphyrin, yielding weaker binding with SWNTs. First principles calculations on the electronic structures further reveal that a distinct charge transfer behavior exists for metallic and semiconducting nanotubes adsorbed with porphyrin that dictates the type-selectivity observed experimentally.[1]

SWNTs are rolled graphene sheets along a certain chiral vector. The structure of a SWNT is uniquely characterized by (n, m) chiral indices. Among chiral vectors, there are two distinctive high-symmetry directions, corresponding to $(n, 0)$ "zig-zag" and (n, n) "armchair." From the rolling graphene model,[9] the chiral angle θ and diameter d_0 of a (n, m) SWNT $(0 \le m \le n)$ are

$$\theta = \arctan\frac{\sqrt{3}m}{2n+m}, \quad d_0 = \frac{\sqrt{3}b}{\pi}\sqrt{n^2+m^2+nm}, \quad (1)$$

respectively, where b is the bond length of graphene. A SWNT is considered to be metallic if $n - m$ is divisible by 3, and semiconducting otherwise. However, the electronic structure of metallic SWNTs is very sensitive to radial deformations because of the presence of degenerate low energy electronic states in these systems.[10] The effect of breaking symmetry due to non-covalent functionalization remains a paucity of classification from first principles calculations.

The SWNTs involved in the present study were constructed based on an sp² hybridization model. The initial value of $b = 1.42$ Å was used. The geometric structures of the SWNTs were fully relaxed in the molecular dynamics through intensive simulated annealing. A systematic evaluation of the available empirical force fields[11] showed that the MM+ and CHARMM force fields provide consistent results for both the carbon nanotubes and porphyrin. In contrast, the COMPASS and AMBER force fields entail difficulties in generating the desired cylindrical configurations of nanotubes. The optimized structures with the use of the MM+ and CHARMM force fields have diameters in good agreement with the predictions from the rolling graphene model,[9] as shown in eqn (1). A porphyrin is an aromatic macrocycle that consists of four pyrrole rings connected by methine bridges.[12] The structural formula of the porphyrin and Zn-porphyrin used in this work are shown in Fig. 1, along with the optimized structures of representative species of THPP or Zn-THPP wrapped around SWNTs.

Department of Physics and Center for Functional Nanoscale Materials, Clark Atlanta University, Atlanta, Georgia 30314, USA. E-mail: xwang@cau.edu
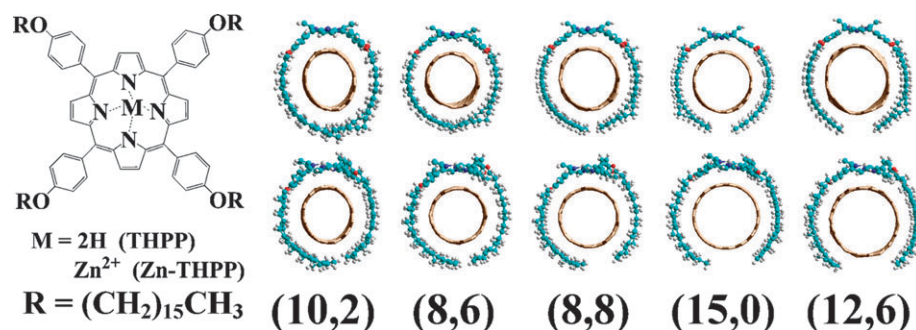
Fig. 1 The structural formula of tetraphenylporphyrin (THPP) and Zn-THPP studied in this work. Top views of the optimized structures using force field-based molecular dynamics are shown in the top and bottom panels, for THPP and Zn-THPP interacting with SWNTs (10,2), (8,6), (8,8), (15,0) and (12,6), respectively.

The binding of the porphyrin to the SWNT is a combination of electrostatic and van der Waals (vdW) interactions. As a consequence, the electrostatic interactions are stronger than vdW binding for non-conjugated molecules, which may explain why the nanotubes are generally dispersed better with conjugated molecules. In general, the adsorption energy can be estimated from the difference between the potential energy of the composite system and the potential energies of the porphyrin and corresponding SWNTs as follows:

$$E = E_{SWNT} + E_{Porphyrin} - E_{total}, \qquad (2)$$

where E_{total} is the total potential energy of the nanohybrid, E_{SWNT} is the energy of the nanotube without the porphyrin and $E_{Porphyrin}$ is the energy of the porphyrin without the nanotube.

We illustrate in Fig. 2 the calculated adsorption energies using force field-based MD. As seen from Fig. 2, the adsorption energy increases with increasing diameter of the tube. This is attributed to an improved geometric match between the planar porphyrin conformation and the carbon nanotube, as well as a reduction in π-orbital misalignment. The THPP-SWNTs (●) have a consistently better adsorption energy compared to those of Zn-THPP-SWNTs (○), with an energy difference of ∼10 kcal mol^{-1}. Closer scrutiny of the optimized structures (see Fig. 1) reveals that the THPP adsorption leads to tighter wrapping around the SWNTs compared to the Zn-THPP adsorption, which is readily observable since the side-chains, $R = (CH_2)_{15}CH_3$, are explicitly included in the calculation. It is worth pointing out that the inclusion of the side chains is not only in accordance with the experiments, but also useful for determining the optimized structure through simulated annealing.

The binding behavior is mainly dependent upon the flattening of the porphyrin macrocycle. The flattening of the macrocycle induces an increase in the π–π interaction area. The present modelling therefore suggests that nanotube solubilization depends strongly upon the geometry of the porphyrin adsorbed onto the SWNT. Specifically, the experimentally observed better solubilization of THPP over Zn-THPP can be interpreted by taking into account the differences in the π–π stacking interactions.[13]
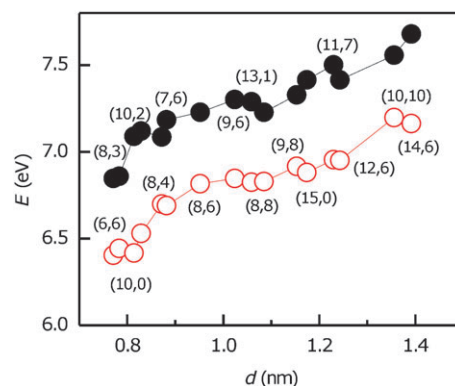
Fig. 2 The calculated adsorption energy dependence on diameter for various species of tube interacting with THPP (●) and Zn-THPP (○), respectively.

The experimental observation of the favorable selection of semiconducting tubes[1] is connected to electronic structures that cannot be assessed through classical force field models. In an effort to understand the electronic properties involved in the type-selectivity, we have performed first principles calculations of five representative SWNTs adsorbed by THPP and Zn-THPP. The calculation is based on density functional theory using the local density approximation of the exchange–correlation potential.[14] All calculations were carried out using a double-numerical basis set.[15] Despite the fact that vdW interactions are not well described in local-density approximations, the computationally-demanding first principles calculation provides important information on level hybridization. Our previous study of the quantum stability of selective enrichment of the helical assembly of flavin mononucleotide wrapping around SWNTs demonstrated that this approach is appropriate for a description of electronic structures.[15]

The structures obtained from force field-based MD calculations were further optimized using the first principles method; the force was converged to less than 0.01 eV Å^{-1}. The structural properties of the optimized conformations are summarized in Table 1. A similar structural trend is observed in force field-based MD calculations. The first principles results from the nanotube diameters are slightly larger than those from the force field-based MD simulations. For the various sizes of tube studied, the porphyrin macrocycle aligns along the tube, and

Table 1 The calculated diameters of the SWNTs wrapped with porphyrin investigated in this work, consisting of three metallic SWNTs, chiral (12,6), zig-zag (15,0) and armchair (8,8), and two semiconducting SWNTs, chiral (8,6) and (10,2). For anisotropic tubes, the maximum and minuend values are shown as d^{MIN} and d^{MAX}. The values from local density functional calculations (d_{LDA}), force field-based MD calculations (d_{MM}) and those of ideal SWNTs (d_0) are shown, together with the molecular formula of THPP- and Zn-THPP-adsorbed SWNTs, the binding energy values from local density functional calculations (E_{LDA}) and force field-based molecular dynamics (E_{MM}), as well as the charge transfer (ΔQ) from THPP to the SWNT

(n, m)	d_{LDA}/nm	d_{MM}/nm	d_0/nm	Molecular formula	E_{LDA}/eV	E_{MM}/eV	ΔQ/e atom^{-1}
(12,6)	1.29	1.26, 1.34	1.243	$C_{444}H_{158}N_4O_4$, $C_{444}H_{156}N_4O_4Zn$	8.89	7.59	1.6×10^{-3}
(15,0)	1.20, 1.25	1.20, 1.24	1.174	$C_{468}H_{158}N_4O_4$, $C_{468}H_{156}N_4O_4Zn$	8.32	7.41	1.7×10^{-3}
(8,8)	1.12, 1.14	1.11, 1.14	1.085	$C_{396}H_{158}N_4O_4$, $C_{396}H_{156}N_4O_4Zn$	8.27	7.11	1.7×10^{-3}
(8,6)	0.99	0.97, 1.01	0.952	$C_{404}H_{158}N_4O_4$, $C_{404}H_{156}N_4O_4Zn$	8.21	7.04	2.1×10^{-3}
(10,2)	0.90, 0.93	0.86, 0.94	0.872	$C_{356}H_{158}N_4O_4$, $C_{356}H_{156}N_4O_4Zn$	8.05	6.87	2.7×10^{-3}

the four pentagons are arranged in such a way that two centers are near the top of the carbon atoms on the SWNT surface while the other two are on top of carbon–carbon bonds. The four alkoxyphenyl rings tilt up at the remote sides away from the macrocycle and the resultant conformation is of a saddle shape. Although there exist local basis corrections for the binding energy calculations,[14–16] the first principles calculation results of the binding energy for the five species are in good agreement with force field-based MD calculation results, especially for the energy orders. An important ramification is that the flattening of the porphyrin macrocycle associated with the reduction of π misalignment is still the predominant factor for the adsorption energy.

The characteristic features of the electronic structure of the THPP-functionalized SWNTs are illustrated by the band structures in Fig. 3, along with those of pristine SWNTs. As seen from Fig. 3, the metallic feature due to the "indirect band overlap" of π and π* states for pristine (8,8) and the semi-metallic states of pristine (12,6) and (15,0) are well reproduced within our calculations. There is a reduction of the band gap for THPP-functionalized semiconducting SWNTs as the HOMO-derived band of the porphyrin intrudes into the gap. On the other hand, for the metallic (8,8), (12,6) and (15,0), there is a paucity of modifications to the bands near the Fermi level. The changes associated with the HOMO-derived band of the porphyrin is consistent with predictions from the charge transfer model.[17] The charge transfer is in the order of 0.002 e atom^{-1} (see Table 1), which is much smaller than that typically found in alkali intercalation experiments.

It is worth noting that functionalized semiconducting and metallic tubes have distinct charge transfer behaviors. For functionalized semiconducting tubes, there is no level hybridization for the HOMO-derived flat band of the porphyrin. The level hybridization and associated charge transfer arise predominantly from the lower valence band derived from the HOMO − 1 orbital of the porphyrin. In contrast, the charge transfer in functionalized metallic tubes is mainly due to the HOMO-derived band of the porphyrin, which causes the splitting of the doubly-degenerate bands for the functionalized (15,0) in the proximity of level hybridization.
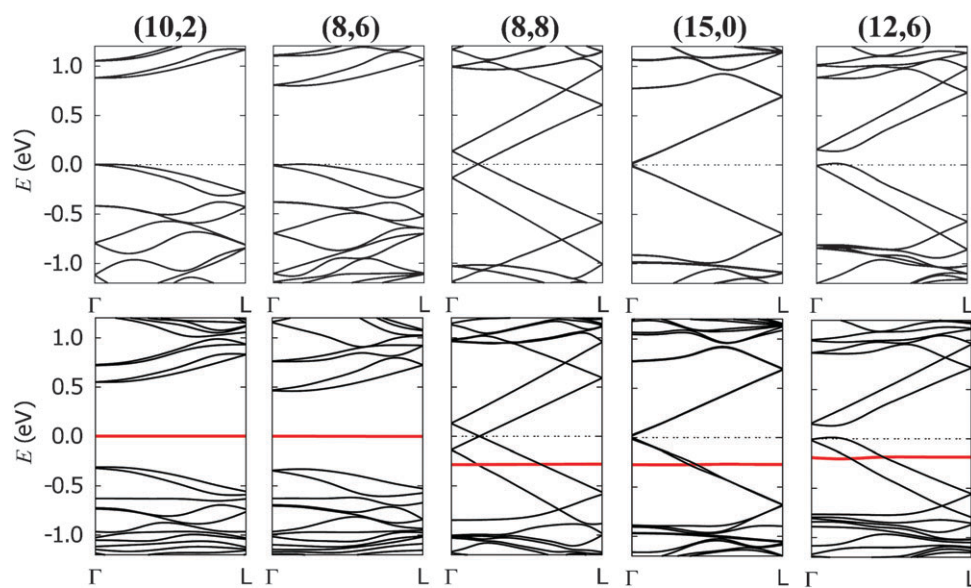
The extracted electronic density distribution for the conduction band maximum (CBM), valence band minimum (VBM) and a few near-gap valence states of THPP adsorbed onto representative semiconducting (10,2) and (8,6), and

metallic (8,8), (12,0) and (12,6) tubes is shown in Fig. 4. In all such cases, the charge density of the CBM is confined to the tube, while that for the VBM depends on the electronic properties of the pristine SWNT. For the functionalized semiconducting tubes, charges of the VBM reside on the THPP macrocycle. In contrast, for metallic tubes, the charges of the VBM accumulate on the SWNT. The distinctive confinement features, observed for each nanotube account for the distinct charge transfer from the porphyrin macrocycle to the semiconducting or metallic nanotube. It is worth noting that for functionalized semiconducting nanotubes, the charge distribution of VBM and CBM is consistent with a type I alignment of the bands.[18–20] However, functionalized metallic nanotubes exhibit a type II alignment. In the latter case, the charge density of the HOMO-derived band of the porphyrin is inhomogeneous due to level hybridization and the associated charge transfer from the porphyrin to the tube. Our results indicate that porphyrins are charge donors to SWNTs, resulting in complete charge separation of the HOMO-derived band of the porphyrin for functionalized semiconducting nanotubes. By way of contrast, for functionalized metallic nanotubes, the charge transfer induces considerable level hybridization, which leads to charged dipoles.[21–25] The charge dipoles, in general, lead to instability with p-doping. This is similar to the issue of stability for nanowires and structures with aromatic residues, which favors structures with a closed electronic shell and homogeneous charge distributions.[19–21,26] As such, we believe that the effects of hole doping and the generated charged dipoles in functionalized metallic SWNTs play an important role in the experimentally observed type-selectivity.

In summary, our calculation results indicate that the semiconducting selectivity can be attributed to the stability of the electronic structure, associated with charge transfer effects. The SWNT–porphyrin bonding is strongly influenced by the adsorption conformation at the nanotube structure, as well as the quantum dipoles associated with charge transfer in metallic tubes. The distinct charge transfer behavior is also expected for a variety of aromatic molecules adsorbed onto SWNTs. The modification of nanotube electronic properties by interacting them with aromatic molecules thus provides a useful means for generating future nanoelectronic devices.

This journal is © The Royal Society of Chemistry and the Centre National de la Recherche Scientifique 2010

Fig. 3 Calculated electronic band structures of pristine (top panels) and functionalized (lower panels) SWNT and THPP nanohybrids for (10,2), (8,6), (8,8), (15,0) and (12,6), respectively. The Fermi level is indicated by the dotted line at $E = 0$ eV. The unit cell along the tube d is about 2 nm, Γ is the band center and $L = \pi/d$. The Fermi level is shifted to 0 eV. The HOMO-derived band of the porphyrin is highlighted. Note that band folding exists that is associated with the long unit cells used in the calculations.
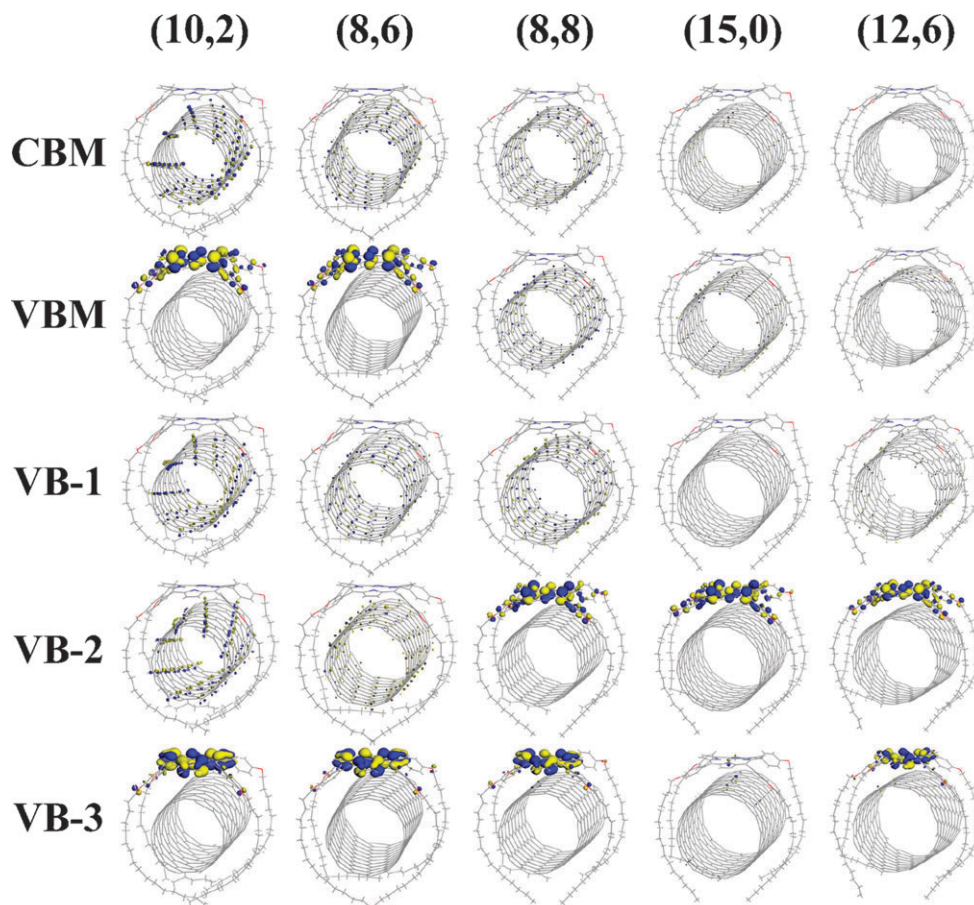
Fig. 4 An isosurface plot of the calculated charge densities for CBM, VBM and a few near-gap valence states of THPP-SWNT complexes. The sign of the wave function is indicated by dark and light grey regions, respectively.

Note and references

1 H. P. Li, B. Zhou, Y. Lin, L. R. Gu, W. Wang, K. A. S. Fernando, S. Kumar, L. F. Allard and Y. P. Sun, *J. Am. Chem. Soc.*, 2004, **126**, 1014–1015.

2 M. Zheng, A. Jagota, E. D. Semke, B. A. Diner, R. S. Mclean, S. R. Lustig, R. E. Richardson and N. G. Tassi, *Nat. Mater.*, 2003, **2**, 338–342.

3 D. W. Steuerman, A. Star, R. Narizzano, H. Choi, R. S. Ries, C. Nicolini, J. F. Stoddart and J. R. Heath, *J. Phys. Chem. B*, 2002, **106**, 3124–3130.

4 H. Murakami, T. Nomura and N. Nakashima, *Chem. Phys. Lett.*, 2003, **378**, 481–485.

5 S.-Y. Ju, J. Doll, I. Sharma and F. Papadimitrakopoulos, *Nat. Nanotechnol.*, 2008, **3**, 356–362.

6 R. R. Johnson, A. T. C. Johnson and M. L. Klein, *Nano Lett.*, 2008, **8**, 69–75.

7 R. J. Chen, Y. Zhang, D. W. Wang and H. J. Dai, *J. Am. Chem. Soc.*, 2001, **123**, 3838–3839.

8 C. S. Lin, R. Q. Zhang, T. A. Niehaus and T. Frauenheim, *J. Phys. Chem. C*, 2007, **111**, 4069–4073.

9 M. Al-Haik, M. Y. Hussaini and H. Garmestani, *J. Appl. Phys.*, 2005, **97**, 074306–074306.

10 P. V. Avramov, K. N. Kudin and G. E. Scuseria, *Chem. Phys. Lett.*, 2003, **370**, 597–601.

11 F. Jensen, *Introduction to Computational Chemistry*, John Wiley & Sons, Hoboken, 2nd edn, 2006, pp. 1–624.

12 S. Pal, A. Datta and S. K. Pati, *Comput. Lett.*, 2007, **3**, 367–372.

13 A. Nish, J. Y. Hwang, J. Doig and R. J. Nicholas, *Nat. Nanotechnol.*, 2007, **2**, 640–646.

14 S. H. Vosko, L. Wilk and M. Nusair, *Can. J. Phys.*, 1980, **58**, 1200–1211.

15 O. O. Ogunro and X.-Q. Wang, *Nano Lett.*, 2009, **9**, 1034–1038.

16 D. K. Samarakoon and X.-Q. Wang, *ACS Nano*, 2009, **3**, 4017–4022.

17 L. Yang and J. Han, *Phys. Rev. Lett.*, 2000, **85**, 154–157.

18 M. Ouyang, J.-L. Huang, C. L. Cheung and C. M. Lieber, *Science*, 2001, **292**, 702–705.

19 A. I. Yanson, I. K. Yanson and J. M. van Ruitenbeek, *Nature*, 2007, **400**, 144–146.

20 A. Nduwimana and X.-Q. Wang, *Nano Lett.*, 2009, **9**, 283–286.

21 A. Nduwimana, R. N. Musin, A. H. Smith and X.-Q. Wang, *Nano Lett.*, 2008, **8**, 3341–3344.

22 I. Jimenez-Fabian, A. de Leon and A. F. Jalbout, *J. Mol. Struct.*, 2008, **849**, 17–22.

23 Q. B. Zheng, Q. Z. Xue, K. O. Yan, L. Z. Hao, Q. Li and X. L. Gao, *J. Phys. Chem. C*, 2007, **111**, 4628–4635.

24 R. Voggu, S. Pal, S. K. Pati and C. N. R. Rao, *J.Phys.: Condens. Matter*, 2008, **20**, 215211–215211.

25 A. K. Manna and S. K. Pati, *Chem.–Asian J.*, 2009, **4**, 855–860.

26 W. Fan, J. Zeng and R.-Q. Zhang, *J. Chem. Theory Comput.*, 2009, **5**, 2879–2885.

This journal is © The Royal Society of Chemistry and the Centre National de la Recherche Scientifique 2010